ACS APPLIED MATERIALS & INTERFACES

Research Article

www.acsami.org

DNA Origami–Graphene Hybrid Nanopore for DNA Detection

Amir Barati Farimani,[†] Payam Dibaeinia,[†] and Narayana R. Aluru*

Department of Mechanical Science and Engineering, Beckman Institute for Advanced Science and Technology, University of Illinois at Urbana–Champaign, Urbana, Illinois 61801, United States

Supporting Information

ABSTRACT: DNA origami nanostructures can be used to functionalize solid-state nanopores for single molecule studies. In this study, we characterized a nanopore in a DNA origami–graphene heterostructure for DNA detection. The DNA origami nanopore is functionalized with a specific nucleotide type at the edge of the pore. Using extensive molecular dynamics (MD) simulations, we computed and analyzed the ionic conductivity of nanopores in heterostructures carpeted with one or two layers of DNA origami on graphene. We demonstrate that a nanopore in DNA origami–graphene gives rise to distinguishable dwell times for the four DNA base types, whereas for a nanopore in bare graphene, the dwell time is almost the same for all types of bases. The specific interactions (hydrogen bonds) between DNA origami and the translocating DNA strand yield different residence times and ionic currents. We also conclude that the speed of DNA translocation decreases due to the friction between the dangling bases at the pore mouth and the sequencing DNA strands.

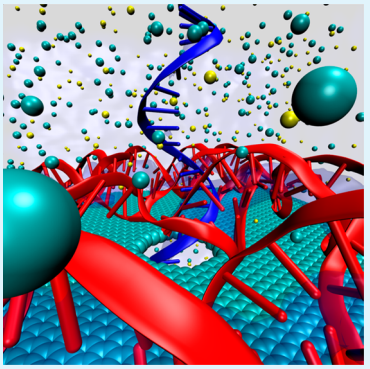

KEYWORDS: *DNA origami, graphene, hybrid nanopore, DNA detection, pore functionalization, multiplex signal, dwell time*

INTRODUCTION

Biological and solid-state nanopores have great potential for DNA sequencing as they provide label-free and fast single-molecule detection.[1,2] In nanopore devices, the ionic current modulated during DNA translocation reveals the nucleotide type.[3,4] Noise in the electric current readout can mask the detection signal, making detection erroneous and difficult.[5−7] To overcome this challenge, practical solutions such as using thin 2D material membranes,[8−16] slowing down DNA translocation,[17−19] employing flexible biological nanopores,[20] pore functionalization, and hybrid nanopores were developed.[21−23] Among these solutions, hybrid nanopores constructed with biological and synthetic materials and chemically and synthetically functionalized pores offer two advantages. First, they can be programmed to yield specific interactions improving the noisy currents or even yielding ancillary detection signals.[24,25] Second, functionalization may be tuned and engineered with nanometer scale precision at the pore mouth.[26,27]

Programmable nanoboxes,[28−32] plates,[24] and channels in bilayers[33,34] are some of the structures constructed using DNA origami techniques. It has been shown that DNA origami[28] can be used for selective detection of biomolecules.[24,35] The self-assembly property and nanometer precision engineering of DNA origami nanostructures are attractive for creating heterostructure and hybrid nanopores.[24,35] Using experimental techniques, DNA origami was inserted into a silicon nitride nanopore and used for detection of λ-DNA.[24] In another work,[24,35] DNA origami nanoplate with some single-stranded DNA (ssDNA) overhangs attached to the pore mouth were deposited on the surface of a solid-state nanopore, and the hybrid nanopore was used for selective detection of proteins and ssDNAs. The "bait–prey" mechanism[24] was used by taking advantage of DNA origami plate on a nanopore to create specific interactions with a translocating target molecule.[24] The specific interactions between the nanopore and the prey molecule increase the translocation time and give rise to a distinguishable signal for selective detection, facilitating single-molecule studies and protein recognition.[36] Molecular dynamics simulations were also used to explore and investigate the stability and structural properties of DNA origami shapes.[37] Recently, the dependence of conductivity on the number of DNA origami layers with different applied biases was characterized.[38] In addition, the packing of origami plates in the presence of Mg^{2+} ions was explored.[38]

With advances in fabrication technologies, deposition and alignment of DNA origami on top of substrates and patterned surfaces,[39−43] chemically modified graphene,[44] and MoS_2[45] are feasible. Considering these advances and the benefits that DNA origami offer to nanopore functionalization,[46] we investigate DNA translocation through a nanopore in a heterostructure of graphene and DNA origami nanoplate. It is notable that molecular scale interactions between DNA origami and translocating DNA are largely unknown. Furthermore, the stability and structure of DNA origami at the pore edge during DNA translocation needs to be understood. In this work, the DNA origami nanopore is functionalized by dangling T bases; i.e., a DNA origami nanopore with unpaired T bases at the edge of the pore is placed on top of a graphene nanopore. In this study, the graphene substrate was primarily used to restrict the

Received: August 31, 2016
Accepted: December 1, 2016
Published: December 1, 2016

DOI: 10.1021/acsami.6b11001
ACS Appl. Mater. Interfaces 2017, 9, 92−100

DNA origami motion under a positive applied bias, even though the electronic structure changes in graphene during DNA translocation can provide additional sensing signals. The sticky behavior of DNA to graphene decreases the movement of DNA origami on top of the graphene and maintains the initial alignment of the nanopores. The (hybrid) nanopores with zero, one and two layers of DNA origami were characterized and used for the detection of DNA bases. The interactions between the hybrid nanopore and translocating DNA, the dwell time of each base type, and the stability of hybrid nanopores were investigated.

METHODS

We performed all-atom molecular dynamics (MD) simulations with NAMD 2.6 using the petascale Blue Waters machine.[47] Visual molecular dynamics (VMD)[48] is used for the visualization of a typical simulation setup consisting of the DNA origami nanoplate, graphene nanopore, ssDNA, water, and ions (~118 000−120 000 atoms, as shown in Figure 1a). A pore with a diameter of 2.1 nm is drilled in the center of a 10 nm × 10 nm single-layer graphene (Figure 1b). In all simulations, the carbon atoms of the graphene sheet inside a ring of radius 1.6 nm around the pore have been restrained by a harmonic potential (with a spring constant of k = 5 kcal/(mol Å^2)), and the remaining atoms of the graphene sheet were fixed.

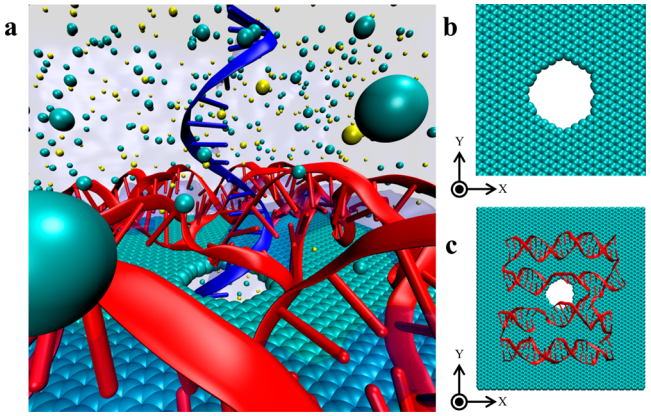

Figure 1. (a) Simulation box consisting of a single-layer DNA origami (depicted in red), graphene sheet, water, ions, and translocating ssDNA (depicted in blue). (b) Bare graphene nanopore. (c) Single-layer DNA origami nanopore on top of a graphene nanopore.

A single layer of 8.7 nm × 9.3 nm × 2.6 nm square lattice DNA origami nanoplate has been designed and generated using caDNAno software.[49] Using caDNAno,[49] the sequence of bases was properly assigned to place a number of A−T base pairs in the middle of the plate. The DNA origami nanoplate is then placed on top of the graphene nanopore. At the location of the graphene pore, the structure of the DNA origami was modified to create an aperture in the DNA origami nanoplate by deleting eight A bases of staple strands and leaving eight unpaired T bases in the scaffold strand. The generated DNA origami pore has roughly a circular shape with a diameter of 1.8 nm. By following the same procedure as for a single-layer DNA origami, a double-layer square lattice DNA origami nanoplate of dimensions 9.0 nm × 11.1 nm × 4.4 nm that includes a semicircular aperture with a diameter of 1.7 nm has also been designed and generated. For the double-layer DNA origami hybrid nanopore, a larger graphene nanoplate that measures 12 nm × 12 nm with a pore diameter of 2.1 nm is used. The dangling unpaired T bases of the DNA origami coat the edge of the graphene nanopore (Figure 1c) (see the Supporting Information for more details on construction of the DNA origami nanopore).

To perform simulations on the translocation of different nucleotide types through the hybrid nanopore with single-layer DNA origami, four different systems were constructed: one for each poly(dA), poly(dC), poly(dG), and poly(dT). Each ssDNA consists of 20 bases. In addition, the same simulation systems were built for translocation of ssDNAs consisting of 30 bases through the double-layer DNA origami hybrid nanopore. In each case, the three first bases of the ssDNA were located inside the hybrid nanopore. Then, the entire structure was solvated in an aqueous 1.0 M NaCl solution.

Water molecules were treated to be rigid using the SHAKE algorithm.[50] The CHARMM27 force field[51] parameters were used for nucleic acids, TIP3P water molecules, graphene, and ions. The periodic boundary condition is applied in all the three directions. The cut-off distance for Lennard-Jones and short-range electrostatic interactions is 12.5 Å. The long-range electrostatic interactions were computed by using the particle−mesh−Ewald (PME) method.[52] The integration time step is 1 fs.

Before equilibration, energy minimization was performed for each system for 25 000 steps. Upon minimization, equilibration was performed for 5 ns with harmonically restrained nucleic acids (for both DNA origami and ssDNA with k_{spring} = 100 kcal/(mol Å^2)). Following that, we maintained the ssDNA with harmonic constraint (with k_{spring} = 1 kcal/(mol Å^2)) and performed equilibration for 2 ns, while the DNA origami nanoplate was free to move with no constraint. Next, another equilibration simulation was performed for 1 ns with no constraint on nucleic acids. All of these equilibration steps were done under NPT ensemble, while pressure was kept constant at 1 atm using the Nosé−Hoover Langevin piston method,[53,54] and the temperature was maintained at the constant value of 300 K by Langevin thermostat.[55] Before applying an external electric field, the system was further equilibrated for 2 ns with NVT ensemble at 300 K.

All ionic current simulations were performed under NVT ensemble at 300 K. An electric field was applied along the z direction (ssDNA axis). During all ionic current simulations, DNA origami nanoplate was completely free to move. The external electric fields are reported in terms of a transmembrane voltage difference $V = -EL_z$, where E is the electric field strength and L_z is the length of the simulation system along the z direction.[56] We monitored the time-dependent ionic current, $I(t)$, through the pore. We computed the ionic current through the nanopore by using the definition of current, $I = dq/dt$, as $I(t) = \frac{1}{L_z}\sum_{i=1}^{n} q_i\left[\frac{z_i(t+\delta t) - z_i(t)}{\delta t}\right]$, where the sum is over all the ions; δt is chosen to be 4 ps; z_i and q_i are the z-coordinate and charge of ion i, respectively; and n is the total number of ions. The ionic current data was block-averaged over intervals of 100 ps.[56]

RESULTS AND DISCUSSION

To characterize the conductivity of hybrid nanopores with one and two layers of DNA origami, single-layer DNA origami, and the bare graphene nanopores, we computed the ionic current associated with these pores for different biases (these systems do not contain translocating ssDNA). For the single-layer DNA origami nanopore case, a graphene sheet with a larger nanopore is used to keep the DNA origami in place because of the applied electric field. Because DNA origami is negatively charged, we did not study the negative branch of the $I-V$ curve as applying negative biases causes the detachment of DNA origami from the surface of the graphene sheet. (See the Supporting Information for detailed studies on detachment of the DNA origami from graphene under negative applied biases). For each bias point in Figure 2a, we performed a simulation for a duration of 40 ns, and we block-averaged the ionic currents over the simulation time. Although the DNA origami has a porous structure that lets ions permeate through (leakage current), in the hybrid nanopores, these porous areas of DNA origami are blocked by the graphene surface. Consequently, the current is primarily due to the ions passing

DOI: 10.1021/acsami.6b11001
ACS Appl. Mater. Interfaces 2017, 9, 92−100

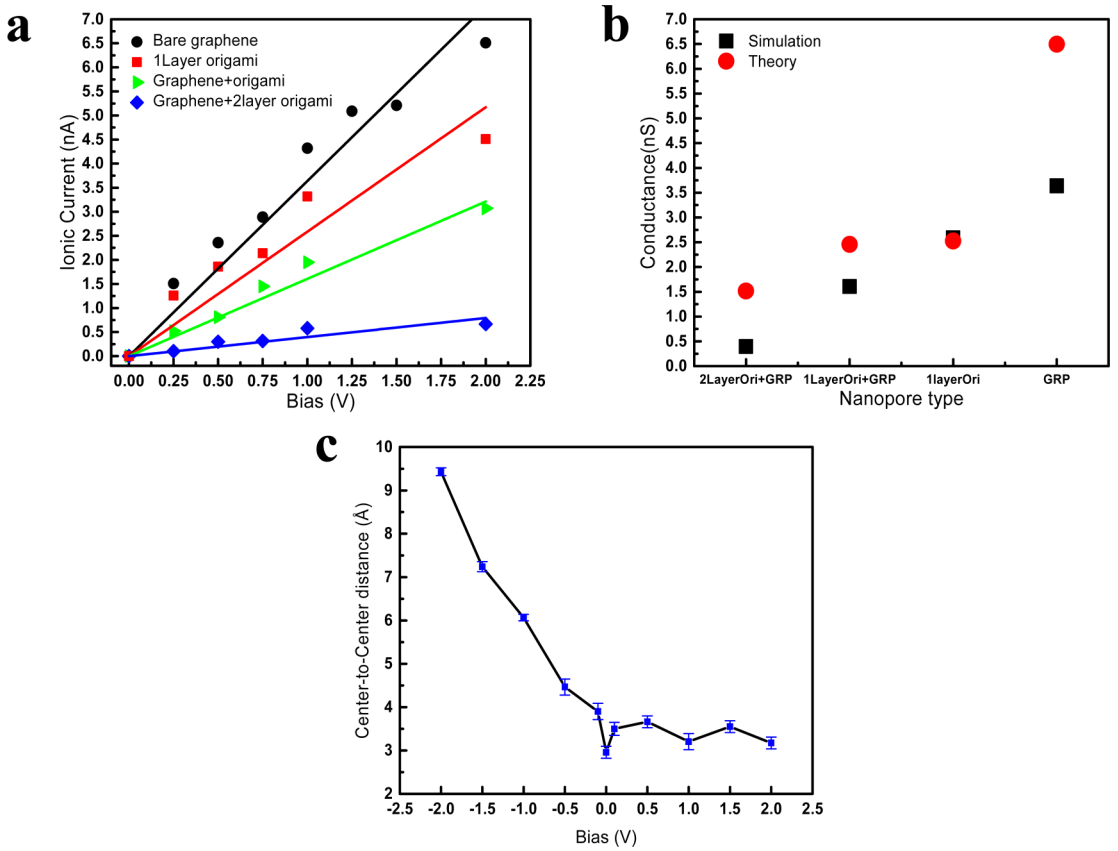

Figure 2. Characteristics of the hybrid nanopores under external biases. (a) $I-V$ curves for the four types of nanopores. Lines are linear fits with the corresponding color for the symbols. (b) Conductance of different pores and their comparison with theoretical predictions. (c) Center-to-center distance of the DNA origami pore to the graphene pore in the $x-y$ plane. Interaction between the DNA origami and the external positive bias does not disarrange the alignment of the hybrid nanopore.

through the pore. In the case of a single-layer DNA origami nanopore, we only accounted for the current through the nanopore of the nanoplate and not through the gaps and free spaces between DNA strands. For the same bias, the bare graphene nanopore has the largest ionic current followed by a single-layer DNA origami nanopore and then the single-layer DNA origami hybrid nanopore followed by the double-layer DNA origami hybrid nanopore (Figure 2a). For a bias of 0.25 V, the currents for double-layer DNA origami hybrid, single-layer DNA origami hybrid, single-layer DNA origami, and bare (pristine) graphene nanopores are 0.104, 0.52, 1.26, and 1.50 nA, respectively (Figure 2a). The characteristic plots for all the pores denote a linear correlation between the current and the applied bias. The resistance of the bare graphene pore is 0.285 V/nA and for the single-layer DNA origami hybrid nanopore is 0.667 V/nA. Because the DNA origami and the graphene nanopores are connected in series, the resistance of the origami nanopore turns out to be 0.382 V/nA (see the Supporting Information for more details on calculating the resistance of the nanopores). The resistances of the hybrid nanopores are higher than the graphene nanopore, which can be attributed to the higher thickness and polarization of the hybrid pores[35,46] (see the Supporting Information to find the $I-V$ curve of single-layer DNA origami hybrid nanopore solvated in 1 M KCl aqueous solution.)

We computed the conductance of each nanopore (Figure 2b). The conductance is defined as $G = I/V$. The highest and lowest conductance is associated with the bare graphene and the double-layer DNA origami hybrid nanopore, respectively. Wannanu et al.[57] proposed the following equation for the conductance

$$G = \kappa\left[\frac{4l_{\mathrm{pore}}}{\pi d^2} + \frac{1}{d}\right]^{-1} \quad (1)$$

where κ is the conductivity of the solution, l_{pore} is the effective thickness of the nanopore, and d is the diameter of the nanopore. The conductivity of the buffer κ is calculated by performing ionic current simulations for a 1 M NaCl solution cell (see the Supporting Information for more details on calculating the conductivity of the buffer). Kowalczyk et al.[58] showed that this model is accurate enough to predict the conductance of nanopores with a thickness of ~8.5 nm, while it overestimates the conductance of thinner membranes.[58] We evaluated and compared the results from eq 1 to our results obtained from MD simulations (Figure 2b). The higher values from eq 1 in comparison with the simulations results can be due to the small thickness of our nanopores. The pore thickness of bare graphene, single-layer DNA origami, single-layer DNA origami hybrid, and double-layer DNA origami hybrid nanopores is 0.34, 2.6, 2.94, and 5.44 nm, respectively.

When an electric field is applied, the DNA origami can move on top of the graphene nanoplate. To characterize the motion of the DNA origami under different biases, we monitored the distance from the center of the graphene pore to the center of the DNA origami pore in the $x-y$ plane for a single-layer DNA origami hybrid nanopore. Figure 2c shows the center-to-center distance averaged over the simulation time for different external

DOI: 10.1021/acsami.6b11001
ACS Appl. Mater. Interfaces 2017, 9, 92−100

biases. Under a positive external bias, the initial alignment of the hybrid nanopore is not significantly changed because the motion of the DNA origami is compensated by the stickiness of DNA origami to graphene. However, under a large negative applied bias, DNA origami detaches from graphene and the interaction between DNA origami and graphene becomes weaker (see the Supporting Information for detailed studies on the detachment of DNA origami from graphene under negative applied biases), and the DNA origami moves on top of the graphene under a negative bias (Figure 2c). The motion of DNA origami under a negative bias can be overcome by sandwiching DNA origami between two graphene nanoplates, i.e., on top and bottom and creating a nanopore in the sandwiched structure (see the Supporting Information for studies on sandwiched DNA origami graphene hybrid nanopore.)

The previous studies[59,60] have shown that by increasing the external bias beyond a critical value, DNA origami can be pulled inside the solid-state nanopore. In our hybrid nanopores, the pores in graphene and DNA origami have almost the same size, and we did not observe any significant pull in phenomenon for external biases below 2 V. In fact, we did not observe pull in phenomenon in our simulations as the DNA strands that are located near the edges of the pore are completely supported by the graphene sheet.

We characterized the instantaneous electrostatic potential map for the distribution of ions, approximated by Gaussian spheres,[61,62] in the single-layer DNA origami hybrid nanopore system under an external bias of 2 V. The instantaneous potential is averaged over 9.5 ns of the simulation time to get the mean resulting transmembrane bias. Figure 3a shows the resulting bias for the system in the $x-z$ plane. The electrostatic potential map near the graphene nanopore is slightly affected by the presence of negatively charged DNA origami. Also, we averaged the total potential over the pore along x and y axes to find the resulting transmembrane bias in the pore along the direction of the external bias, i.e., the z axis (Figure 3b). This plot shows that the potential drops primarily across the nanopore from zero to −2 V and does not change significantly in the electrolyte (far from the nanopore).

The presence of the T bases at the mouth of the pore induces specific interactions with the translocating DNA, especially with its complementary base, i.e., base A. These interactions usually lower the ssDNAs translocation speed and give rise to specific signatures for DNA detection. To investigate the translocation speed of ssDNA in hybrid nanopores and bare graphene, we simulated a poly$(dA)_{20}$ in a bare graphene nanopore (Figure 4a), 4 poly ssDNAs with 20 bases (A, C, G, and T bases) in single-layer and double-layer DNA origami hybrid nanopores (Figure 4b,c). All of these simulations were performed for a bias of 2.0 V. The most rapid electrophoretic translocation is observed for the bare graphene nanopore, in which 20 DNA bases (type A) passed through the pore in 5 ns (Figure 4d). The lowest translocation is observed for poly$(dA)_{30}$ through the double-layer DNA origami hybrid nanopore, in which only five bases translocated in 26 ns (Figure 4e). For the single-layer DNA origami hybrid nanopore, poly$(dG)_{20}$ has the fastest translocation speed followed by poly$(dC)_{20}$ and poly$(dT)_{20}$, and poly$(dA)_{20}$ has the smallest translocation speed. For poly$(dA)_{20}$, only 15 bases successfully translocated, and the five last bases were stuck in the pore for more than 30 ns. All the base types reside in the double-layer DNA origami hybrid nanopore for a longer time compared to

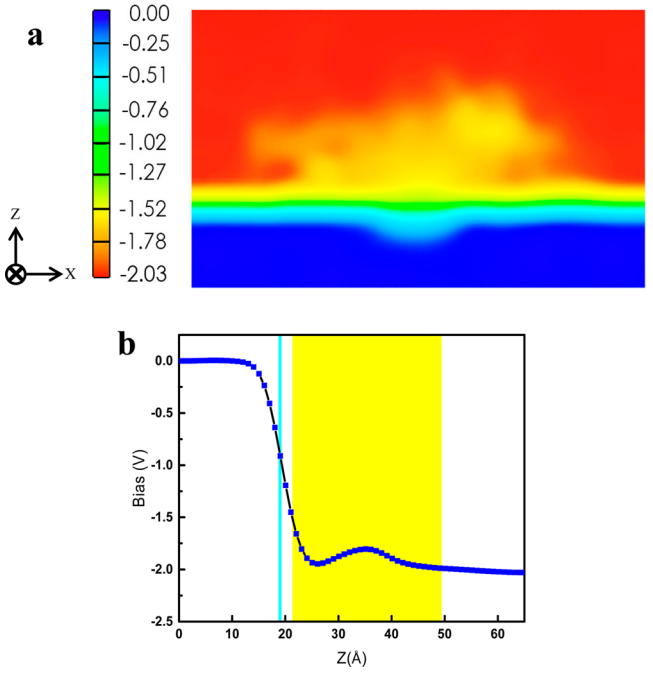

Figure 3. (a) Electrostatic potential map of the single-layer DNA origami hybrid nanopore under an external applied bias of 2 V. Ions and other point charges are approximated by Gaussian spheres with an inverse width of $\beta = 0.25$ Å^{-1}. (b) The resulting mean bias across the pore along the z direction, averaged over x and y directions. The cyan and yellow regions approximately show, respectively, the area where the graphene nanopore and the DNA origami nanopore occupy along the z direction during the simulation time. The potential is primarily changing across the graphene nanopore.

the single-layer DNA origami hybrid nanopore although the capture of A bases is still more stable compared to the other base types (Figure 4e).

To find the statistical distribution of dwell times, we performed 20 simulations for each translocating ssDNA type, poly$(dA)_{20}$, poly$(dC)_{20}$, poly$(dG)_{20}$, and poly$(dT)_{20}$ (80 simulations in total), through a single-layer DNA origami hybrid nanopore under an external bias of 2 V with different initial velocities and a total simulation time of ∼1.2 μs. Figure 4f shows that most of the A bases reside inside the pore for longer times compared to the other base types. The expected value of the residence time of base type A is approximately 3 ns, and for base types C, G, and T is 1.6, 0.75, and 0.64 ns, respectively. Although the nonhybridized dangling bases of DNA origami nanopore only allow for efficient interactions with A bases, C bases also have long residence time compared to G and T bases. The reason can be explained by the overall (VdW and electrostatic) interactions between ssDNA and nanopore especially the instantaneous hydrogen bonding between poly(dC) and G bases of G−C base pairs near the nanopore. These interactions are a result of the specific configuration of DNA origami base pairs (see the Supporting Information for detailed studies about the interactions between ssDNAs and nanopore). We also averaged the residence time of bases at the pore mouth and found that the A base resides in the single-layer DNA origami hybrid nanopore about nine times longer than in the bare graphene nanopore (Figure 4g). Furthermore, in the case of single-layer DNA origami hybrid nanopore, A bases dwell in the pore about two times longer than T and C and three times longer than G (Figure 4g). While

DOI: 10.1021/acsami.6b11001
ACS Appl. Mater. Interfaces 2017, 9, 92−100

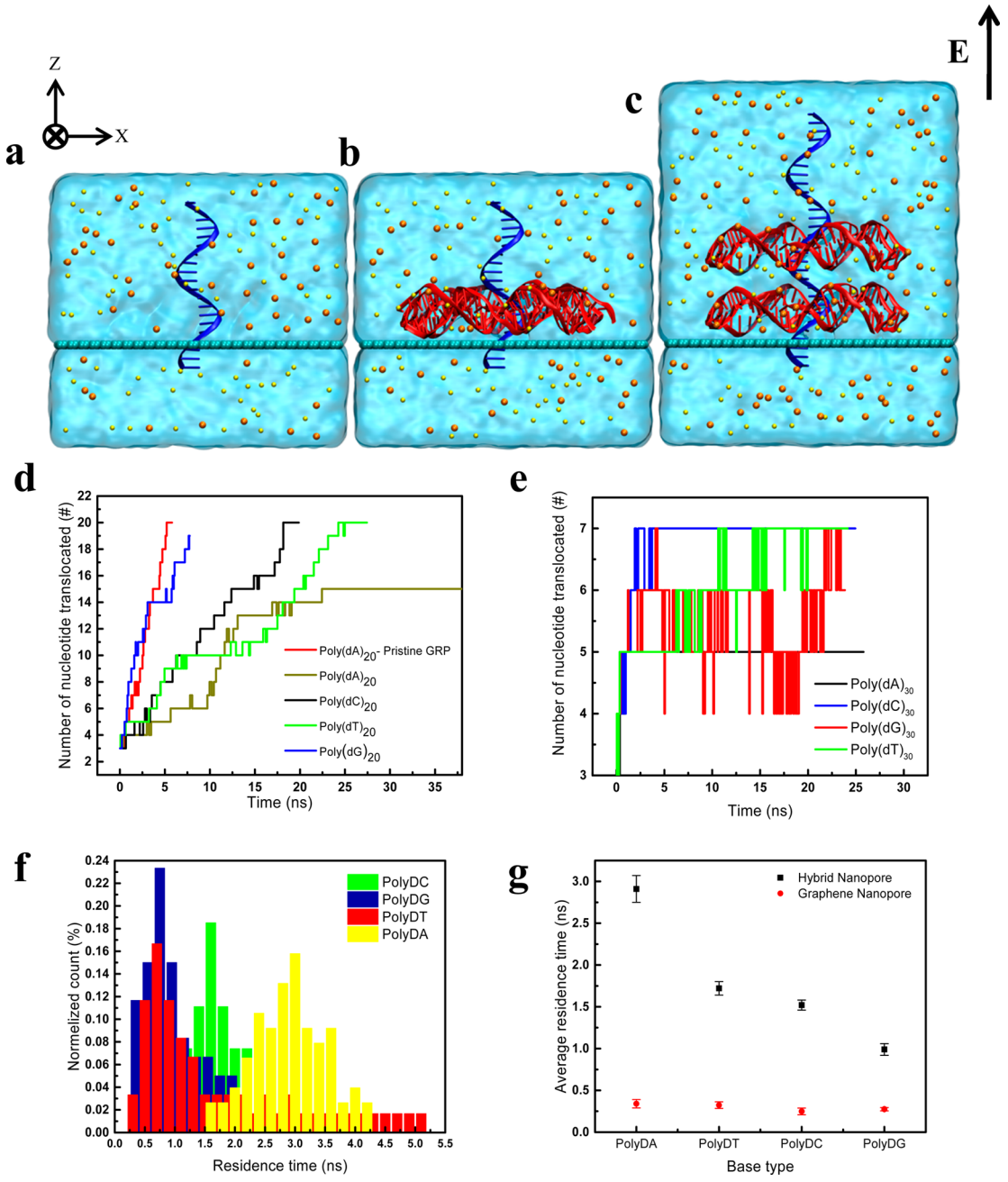

Figure 4. (a) Simulation system of DNA translocating through a bare graphene nanopore. The all-atom model contains a graphene nanopore, ssDNA (depicted in blue), water, and ions. (b) Simulation system of DNA translocating through a single-layer DNA origami hybrid nanopore. The all-atom model contains a single-layer DNA origami (depicted in red)−graphene nanopore, ssDNA (depicted in blue), water, and ions. (c) Simulation system of DNA translocating through a double-layer DNA origami hybrid nanopore. The all-atom model contains a double-layer DNA origami (depicted in red)−graphene nanopore, ssDNA (depicted in blue), water, and ions. (d) Translocation history of ssDNA in pristine graphene and single-layer DNA origami hybrid nanopores. (e) Translocation history of ssDNA in double-layer DNA origami hybrid nanopore. (f) Statistical distribution of the dwell times for different base types translocating through single-layer DNA origami hybrid nanopore under an external bias of 2 V. (g) Average residence time of base in single-layer DNA origami hybrid and bare graphene nanopores.

the residence time of different base types is nearly the same for the graphene nanopore, it varies significantly depending on the base type translocating through the hybrid nanopore. This feature of the hybrid nanopore can be used as an ancillary detection signal for DNA base sensing. Although the dwell time can help distinguish the signal, it cannot be a standalone signature for detection (specifically, if the levels of currents for each base are close to each other).

To obtain more insight into the interactions between the hybrid pore and the translocating DNA strand, we computed the average number of hydrogen bonds (HB) between ssDNA and DNA origami in the nanopore region for the single-layer DNA origami hybrid nanopore. The snapshots of hydrogen bonding during translocation of DNA are shown in Figure 5a,b. The bases of poly$(dA)_{20}$ create the largest number of hydrogen bonds with the DNA origami, while the bases of poly$(dT)_{20}$ have the smallest number of hydrogen bonds during the

DOI: 10.1021/acsami.6b11001
ACS Appl. Mater. Interfaces 2017, 9, 92−100

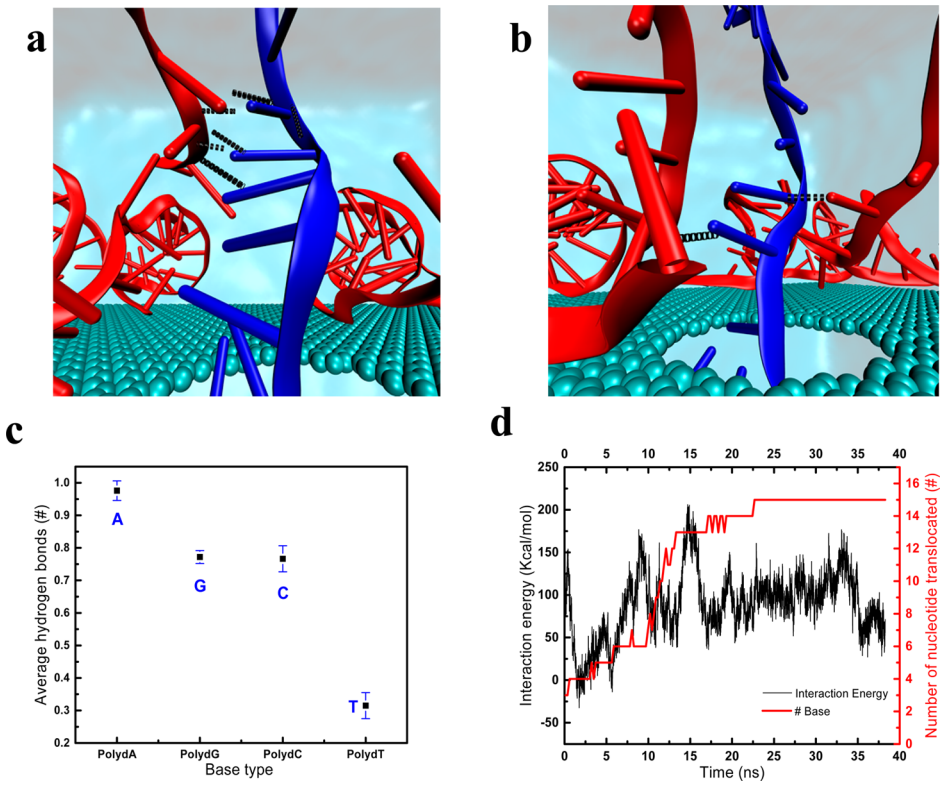

Figure 5. (a) Snapshot of hydrogen bonds between poly(dA) and DNA origami (the black dashed lines represent HBs). (b) Snapshot of hydrogen bonds between poly(dT) and DNA origami (the black dashed lines represent HBs). (c) Average number of HBs between ssDNA and DNA origami nanoplates. (d) Time-dependent interaction energy between poly(dA) and DNA origami nanoplate (black). Translocation plot of poly(dA) through hybrid nanopore (red).

simulation time. Bases of poly(dC)$_{20}$ and poly(dG)$_{20}$ create almost the same number of hydrogen bonds during the simulation time (Figure 5c). The A (translocating base type)−T (unpaired dangling bases of the pore) base pairing gives rise to the highest attraction between poly(dA)$_{20}$ and the hybrid nanopore and the highest number of HBs. However, for translocation of poly(dT), we observed the lowest number of HBs because of the mismatch between ssDNA T bases and the unpaired dangling T bases of the pore (Figure 5c).

To understand the change in the interaction energy during translocation of ssDNA, we computed the interaction energy between the atoms of the translocating poly(dA) and the DNA origami nanoplate in the single-layer DNA origami hybrid nanopore (Figure 5d). There is a high correlation between the interaction energy and the stepwise translocation history (Figure 5d). For example, some bases were stuck in the time window of 7−10 and 14−16 ns (long-lasting flat steps are the signatures of bases being stuck; Figure 5d), and at the same time, we observed a peak (local maxima) in the interaction energy (190 and 210 kcal/mol, respectively). In other words, at time instances in which the DNA origami and the translocating DNA are strongly interacting with each other, the electrophoretic forces could not overcome the friction between the DNA origami and the translocating DNA, which gives rise to a higher residence time. At the time instances in which successive translocation occurs, the average of interaction energies is lower and around 110 kcal/mol.

Figure 6a illustrates the schematic of the system used for ionic current simulations. To explore the ionic current characteristic of the single-layer DNA origami hybrid nanopore, we averaged the current associated with the translocation of each poly ssDNA type (Figure 6b). Bases A and G are distinguishable by their ionic currents, while for bases C and T, the ionic currents are about the same (Figure 6b). In measurements with the nanopore technology, the translocation of DNA chain is performed hundreds of times and the ionic current and the dwell time (bandwidth) of each translocation event are recorded. The combination of dwell time and ionic current in the statistical distribution (data clusters built upon dwell time and ionic current for each base) are used to distinguish nucleotides.

To understand the stability and arrangement of the dangling unpaired T bases at the pore entrance, we monitored the number of bases of DNA origami nanoplate, which reside around the pore for the translocation of poly(dA)$_{20}$ through the single-layer DNA origami hybrid nanopore (see the Supporting Information for translocation of other poly ssDNAs). The geometrical space that we examined the bases is within an infinitely long cylinder concentric with the pore center and with a radius of 22.4 Å. The most-prevalent base type of the DNA origami nanoplate around the pore is T, which resides around the pore in a stable manner (Figure 6c). The number of the other base types (i.e., A, C, and G) prevalent at the pore vicinity is approximately one-third of the number of base type T, which implies that the initially functionalized DNA origami with unpaired T bases is stable even in the presence of thermal noise, water and ion permeation, and DNA electrophoretic translocation (Figure 6c).

To investigate the status of pore functionalization during the translocation of other poly ssDNAs, we averaged the number of different base types of the DNA origami residing in the geometrical space, as defined above, over the entire period of

DOI: 10.1021/acsami.6b11001
ACS Appl. Mater. Interfaces 2017, 9, 92−100

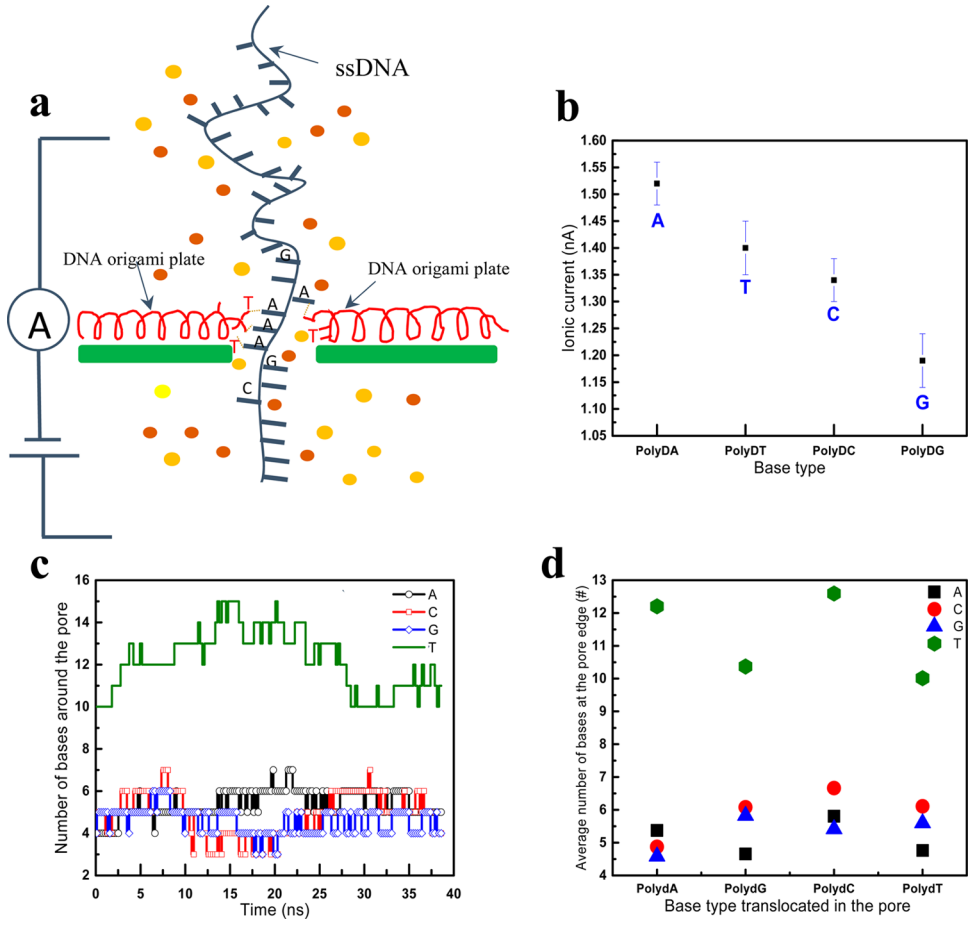

Figure 6. (a) Schematic of the ionic current simulation system showing the interaction of the complementary bases (A–T). (b) Ionic currents for different bases computed from the translocation of poly ssDNAs through the single-layer DNA origami hybrid nanopore. (c) Density of different bases of the DNA origami nanoplate in the vicinity of the pore vs simulation time for translocation of poly(dA) through the single-layer DNA origami hybrid nanopore. (d) Average density of different bases of the DNA origami nanoplate in the vicinity of the pore during poly ssDNAs translocations through the single-layer DNA origami hybrid nanopore.

DNA translocation (Figure 6d). A total of 10–13 T bases reside around the pore, but only 4–6 bases of A, C, and G types stay near the pore. Interestingly, bases of poly(dA) and poly(dC) attract the T bases of DNA origami nanoplate more than poly(dG) and poly(dT) do (Figure 6d, green line). As a result, more number of T bases of DNA origami line the pore during the simulation of poly(dA) and poly(dC). For the translocation of A bases, the higher number of hydrogen bonds combined with the high density of complementary T bases around the pore create specific interactions resulting in a higher dwell time for base A.

The higher residence time of the single base at the pore would be beneficial for DNA read-out. Longer residence time and slower speed of DNA translocation can ensure a higher resolution signal acquisition. In nanopores, usually, the speed of translocation is fast even at low biases of around 100 mV that the MHz bandwidth of current amplifiers may not be able to resolve the single base readouts. Among the solutions that were proposed for speed reduction are the use of high-viscosity buffer solution,[17] lower temperature,[63] flexible MscL nanopores,[20] pore functionalization,[64] and ionic liquid systems.[65] The presence of DNA origami on top of a graphene nanopore not only creates an additional signature for recognition but also reduces the speed of translocation. To quantify and compare the speed of translocation of poly(dA) in hybrid and bare graphene nanopores, we performed simulations of up to 70 ns at different biases (Figure 7). At biases between 2 and 4 V, the translocation rate for the hybrid pore is 5–7 times slower than that for the bare graphene pore (Figure 7). At lower biases, DNA bases reside for a longer time inside the pore, and hence,

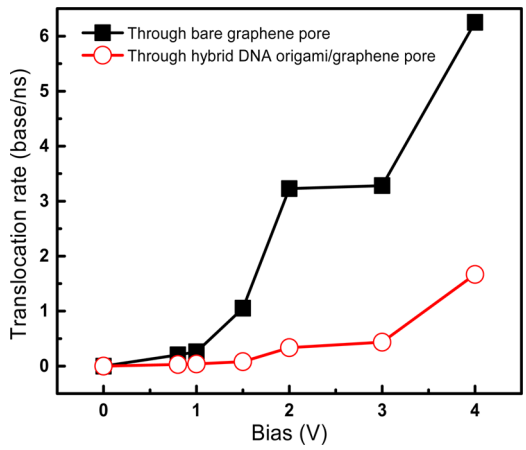

Figure 7. Comparison of poly(dA) translocation rate through the single-layer DNA origami hybrid nanopore and the bare graphene nanopore.

DOI: 10.1021/acsami.6b11001
ACS Appl. Mater. Interfaces 2017, 9, 92–100

the probability increases to form hydrogen bond with the hybrid pore. This gives rise to a longer dwell time.

CONCLUSIONS

We demonstrated that the hybrid DNA origami−graphene nanopore can yield a distinguishable dwell time for DNA bases. A total of four different nanopores (i.e., bare graphene, single-layer DNA origami, single-layer DNA origami hybrid, and double-layer DNA origami hybrid nanopores) were characterized in terms of ionic current, conductance, and resistance. The functionalization of a DNA origami nanopore with T bases remains intact during the electrophoretic translocation of ssDNA bases. The combination of distinguishable dwell time and ionic current along with the slower speed of translocation make the hybrid DNA origami−graphene nanopore attractive for selective DNA detection. The hydrogen bonds between translocating ssDNA and DNA origami at the pore contribute to the distinguishable dwell time.

ASSOCIATED CONTENT

Supporting Information

The Supporting Information is available free of charge on the ACS Publications website at DOI: 10.1021/acsami.6b11001.

Calculation of resistivity and conductivity of different nanopore architectures, the design and structure of single-layer and double-layer DNA origami nanopore, density of bases around the pore mouth, motion of DNA origami on top of graphene under external biases, sandwiched DNA origami−graphene hybrid nanopore analysis and *I*−*V* curve of hybrid nanopore solvated in 1 M KCl aqueous solution. (PDF)

AUTHOR INFORMATION

Corresponding Author

*E-mail: aluru@illinois.edu.

ORCID

Amir Barati Farimani: 0000-0002-2952-8576

Author Contributions

†A.B.F. and P.D. contributed equally to this work

Notes

The authors declare no competing financial interest.

ACKNOWLEDGMENTS

This work is supported by AFOSR under grant no. FA9550-12-1-0464 and by NSF under grant nos. 1264282, 1420882, 1506619, and 1545907. The authors gratefully acknowledge the use of the parallel computing resource Blue Waters provided by the University of Illinois and the National Center for Supercomputing Applications (NCSA).

REFERENCES

(1) Venkatesan, B. M.; Bashir, R. Nanopore Sensors for Nucleic Acid Analysis. *Nat. Nanotechnol.* **2011**, *6*, 615−624.

(2) Keyser, U. F. Controlling Molecular Transport through Nanopores. *J. R. Soc., Interface* **2011**, *8*, 1369−1378.

(3) Kasianowicz, J. J.; Brandin, E.; Branton, D.; Deamer, D. W. Characterization of Individual Polynucleotide Molecules Using a Membrane Channel. *Proc. Natl. Acad. Sci. U. S. A.* **1996**, *93*, 13770−13773.

(4) Bayley, H.; Cremer, P. S. Stochastic Sensors Inspired by Biology. *Nature* **2001**, *413*, 226−230.

(5) Deamer, D. W.; Branton, D. Characterization of Nucleic Acids by Nanopore Analysis. *Acc. Chem. Res.* **2002**, *35*, 817−825.

(6) Dekker, C. Solid-State Nanopores. *Nat. Nanotechnol.* **2007**, *2*, 209−215.

(7) Branton, D.; Deamer, D. W.; Marziali, A.; Bayley, H.; Benner, S. A.; Butler, T.; Di Ventra, M.; Garaj, S.; Hibbs, A.; Huang, X. H.; Jovanovich, S. B.; Krstic, P. S.; Lindsay, S.; Ling, X. S. S.; Mastrangelo, C. H.; Meller, A.; Oliver, J. S.; Pershin, Y. V.; Ramsey, J. M.; Riehn, R.; Soni, G. V.; Tabard-Cossa, V.; Wanunu, M.; Wiggin, M.; Schloss, J. A. The Potential and Challenges of Nanopore Sequencing. *Nat. Biotechnol.* **2008**, *26*, 1146−1153.

(8) Farimani, A. B.; Min, K.; Aluru, N. R. DNA Base Detection Using a Single-Layer MoS2. *ACS Nano* **2014**, *8*, 7914−22.

(9) Liu, K.; Feng, J. D.; Kis, A.; Radenovic, A. Atomically Thin Molybdenum Disulfide Nanopores with High Sensitivity for DNA Trans Location. *ACS Nano* **2014**, *8*, 2504−2511.

(10) Schneider, G. F.; Kowalczyk, S. W.; Calado, V. E.; Pandraud, G.; Zandbergen, H. W.; Vandersypen, L. M. K.; Dekker, C. DNA Translocation through Graphene Nanopores. *Nano Lett.* **2010**, *10*, 3163−3167.

(11) Traversi, F.; Raillon, C.; Benameur, S. M.; Liu, K.; Khlybov, S.; Tosun, M.; Krasnozhon, D.; Kis, A.; Radenovic, A. Detecting the Translocation of DNA through a Nanopore Using Graphene Nanoribbons. *Nat. Nanotechnol.* **2013**, *8*, 939−945.

(12) Saha, K. K.; Drndic, M.; Nikolic, B. K. DNA Base-Specific Modulation of Microampere Transverse Edge Currents through a Metallic Graphene Nanoribbon with a Nanopore. *Nano Lett.* **2012**, *12*, 50−55.

(13) Merchant, C. A.; Healy, K.; Wanunu, M.; Ray, V.; Peterman, N.; Bartel, J.; Fischbein, M. D.; Venta, K.; Luo, Z. T.; Johnson, A. T. C.; Drndic, M. DNA Translocation through Graphene Nanopores. *Nano Lett.* **2010**, *10*, 2915−2921.

(14) Merchant, C. A.; Drndic, M. Graphene Nanopore Devices for DNA Sensing. *Methods Mol. Biol. (N. Y., NY, U. S.)* **2012**, *870*, 211−226.

(15) Heerema, S. J.; Dekker, C. Graphene Nanodevices for DNA Sequencing. *Nat. Nanotechnol.* **2016**, *11*, 127−136.

(16) Garaj, S.; Liu, S.; Golovchenko, J. A.; Branton, D. Molecule-Hugging Graphene Nanopores. *Proc. Natl. Acad. Sci. U. S. A.* **2013**, *110*, 12192−12196.

(17) Fologea, D.; Uplinger, J.; Thomas, B.; McNabb, D. S.; Li, J. L. Slowing DNA Translocation in a Solid-State Nanopore. *Nano Lett.* **2005**, *5*, 1734−1737.

(18) Kowalczyk, S. W.; Wells, D. B.; Aksimentiev, A.; Dekker, C. Slowing Down DNA Translocation through a Nanopore in Lithium Chloride. *Nano Lett.* **2012**, *12*, 1038−1044.

(19) Wanunu, M.; Sutin, J.; McNally, B.; Chow, A.; Meller, A. DNA Translocation Governed by Interactions with Solid-State Nanopores. *Biophys. J.* **2008**, *95*, 4716−4725.

(20) Farimani, A. B.; Heiranian, M.; Aluru, N. R. Electromechanical Signatures for DNA Sequencing through a Mechanosensitive Nanopore. *J. Phys. Chem. Lett.* **2015**, *6*, 650−657.

(21) Luan, B. Q.; Stolovitzky, G.; Martyna, G. Slowing and Controlling the Translocation of DNA in a Solid-State Nanopore. *Nanoscale* **2012**, *4*, 1068−1077.

(22) Butler, T. Z.; Pavlenok, M.; Derrington, I. M.; Niederweis, M.; Gundlach, J. H. Single-Molecule DNA Detection with an Engineered Mspa Protein Nanopore. *Proc. Natl. Acad. Sci. U. S. A.* **2008**, *105*, 20647−20652.

(23) Sint, K.; Wang, B.; Kral, P. Selective Ion Passage through Functionalized Graphene Nanopores. *J. Am. Chem. Soc.* **2008**, *130*, 16448−16449.

(24) Wei, R. S.; Martin, T. G.; Rant, U.; Dietz, H. DNA Origami Gatekeepers for Solid-State Nanopores. *Angew. Chem., Int. Ed.* **2012**, *51*, 4864−4867.

(25) Yusko, E. C.; Johnson, J. M.; Majd, S.; Prangkio, P.; Rollings, R. C.; Li, J. L.; Yang, J.; Mayer, M. Controlling Protein Translocation through Nanopores with Bio-Inspired Fluid Walls. *Nat. Nanotechnol.* **2011**, *6*, 253−260.

DOI: 10.1021/acsami.6b11001
ACS Appl. Mater. Interfaces 2017, 9, 92−100

(26) Martin, C. R.; Siwy, Z. S. Learning Nature's Way: Biosensing with Synthetic Nanopores. *Science* **2007**, *317*, 331−332.
(27) Iqbal, S. M.; Akin, D.; Bashir, R. Solid-State Nanopore Channels with DNA Selectivity. *Nat. Nanotechnol.* **2007**, *2*, 243−248.
(28) Rothemund, P. W. K. Folding DNA to Create Nanoscale Shapes and Patterns. *Nature* **2006**, *440*, 297−302.
(29) Andersen, E. S.; Dong, M.; Nielsen, M. M.; Jahn, K.; Subramani, R.; Mamdouh, W.; Golas, M. M.; Sander, B.; Stark, H.; Oliveira, C. L. P.; Pedersen, J. S.; Birkedal, V.; Besenbacher, F.; Gothelf, K. V.; Kjems, J. Self-Assembly of a Nanoscale DNA Box with a Controllable Lid. *Nature* **2009**, *459*, 73−75.
(30) Sobczak, J. P. J.; Martin, T. G.; Gerling, T.; Dietz, H. Rapid Folding of DNA into Nanoscale Shapes at Constant Temperature. *Science* **2012**, *338*, 1458−1461.
(31) Falconi, M.; Oteri, F.; Chillemi, G.; Andersen, F. F.; Tordrup, D.; Oliveira, C. L. P.; Pedersen, J. S.; Knudsen, B. R.; Desideri, A. Deciphering the Structural Properties That Confer Stability to a DNA Nanocage. *ACS Nano* **2009**, *3*, 1813−1822.
(32) Zadegan, R. M.; Jepsen, M. D. E.; Thomsen, K. E.; Okholm, A. H.; Schaffert, D. H.; Andersen, E. S.; Birkedal, V.; Kjems, J. Construction of a 4 Zeptoliters Switchable 3d DNA Box Origami. *ACS Nano* **2012**, *6*, 10050−10053.
(33) Langecker, M.; Arnaut, V.; Martin, T. G.; List, J.; Renner, S.; Mayer, M.; Dietz, H.; Simmel, F. C. Synthetic Lipid Membrane Channels Formed by Designed DNA Nanostructures. *Science* **2012**, *338*, 932−936.
(34) Seifert, A.; Gopfrich, K.; Burns, J. R.; Fertig, N.; Keyser, U. F.; Howorka, S. Bilayer-Spanning DNA Nanopores with Voltage-Switching between Open and Closed State. *ACS Nano* **2015**, *9*, 1117−1126.
(35) Hernandez-Ainsa, S.; Bell, N. A. W.; Thacker, V. V.; Gopfrich, K.; Misiunas, K.; Fuentes-Perez, M. E.; Moreno-Herrero, F.; Keyser, U. F. DNA Origami Nanopores for Controlling DNA Translocation. *ACS Nano* **2013**, *7*, 6024−6030.
(36) Wei, R. S.; Gatterdam, V.; Wieneke, R.; Tampe, R.; Rant, U. Stochastic Sensing of Proteins with Receptor-Modified Solid-State Nanopores. *Nat. Nanotechnol.* **2012**, *7*, 257−263.
(37) Yoo, J.; Aksimentiev, A. In Situ Structure and Dynamics of DNA Origami Determined through Molecular Dynamics Simulations. *Proc. Natl. Acad. Sci. U. S. A.* **2013**, *110*, 20099−20104.
(38) Li, C. Y.; Hemmig, E. A.; Kong, J. L.; Yoo, J.; Hernandez-Ainsa, S.; Keyser, U. F.; Aksimentiev, A. Ionic Conductivity, Structural Deformation, and Programmable Anisotropy of DNA Origami in Electric Field. *ACS Nano* **2015**, *9*, 1420−1433.
(39) Gao, B.; Sarveswaran, K.; Bernstein, G. H.; Lieberman, M. Guided Deposition of Individual DNA Nanostructures on Silicon Substrates. *Langmuir* **2010**, *26*, 12680−12683.
(40) Teshome, B.; Facsko, S.; Keller, A. Topography-Controlled Alignment of DNA Origami Nanotubes on Nanopatterned Surfaces. *Nanoscale* **2014**, *6*, 1790−1796.
(41) Pearson, A. C.; Pound, E.; Woolley, A. T.; Linford, M. R.; Harb, J. N.; Davis, R. C. Chemical Alignment of DNA Origami to Block Copolymer Patterned Arrays of 5 Nm Gold Nanoparticles. *Nano Lett.* **2011**, *11*, 1981−1987.
(42) Gu, H. Z.; Chao, J.; Xiao, S. J.; Seeman, N. C. Dynamic Patterning Programmed by DNA Tiles Captured on a DNA Origami Substrate. *Nat. Nanotechnol.* **2009**, *4*, 245−248.
(43) Kershner, R. J.; Bozano, L. D.; Micheel, C. M.; Hung, A. M.; Fornof, A. R.; Cha, J. N.; Rettner, C. T.; Bersani, M.; Frommer, J.; Rothemund, P. W. K.; Wallraff, G. M. Placement and Orientation of Individual DNA Shapes on Lithographically Patterned Surfaces. *Nat. Nanotechnol.* **2009**, *4*, 557−561.
(44) Yun, J. M.; Kim, K. N.; Kim, J. Y.; Shin, D. O.; Lee, W. J.; Lee, S. H.; Lieberman, M.; Kim, S. O. DNA Origami Nanopatterning on Chemically Modified Graphene. *Angew. Chem., Int. Ed.* **2012**, *51*, 912−915.
(45) Zhang, X. N.; Rahman, M.; Neff, D.; Norton, M. L. DNA Origami Deposition on Native and Passivated Molybdenum Disulfide Substrates. *Beilstein J. Nanotechnol.* **2014**, *5*, 501−506.
(46) Bell, N. A. W.; Keyser, U. F. Nanopores Formed by DNA Origami: A Review. *FEBS Lett.* **2014**, *588*, 3564−3570.
(47) Kale, L.; Skeel, R.; Bhandarkar, M.; Brunner, R.; Gursoy, A.; Krawetz, N.; Phillips, J.; Shinozaki, A.; Varadarajan, K.; Schulten, K. Namd2: Greater Scalability for Parallel Molecular Dynamics. *J. Comput. Phys.* **1999**, *151*, 283−312.
(48) Humphrey, W.; Dalke, A.; Schulten, K. Vmd: Visual Molecular Dynamics. *J. Mol. Graphics* **1996**, *14*, 33−38.
(49) Douglas, S. M.; Marblestone, A. H.; Teerapittayanon, S.; Vazquez, A.; Church, G. M.; Shih, W. M. Rapid Prototyping of 3d DNA-Origami Shapes with Cadnano. *Nucleic Acids Res.* **2009**, *37*, 5001−5006.
(50) Ryckaert, J. P.; Ciccotti, G.; Berendsen, H. J. C. Numerical-Integration of Cartesian Equations of Motion of a System with Constraints - Molecular-Dynamics of N-Alkanes. *J. Comput. Phys.* **1977**, *23*, 327−341.
(51) MacKerell, A. D.; Banavali, N. K. All-Atom Empirical Force Field for Nucleic Acids: Ii. Application to Molecular Dynamics Simulations of DNA and Rna in Solution. *J. Comput. Chem.* **2000**, *21*, 105−120.
(52) Darden, T.; York, D.; Pedersen, L. Particle Mesh Ewald - an N.Log(N) Method for Ewald Sums in Large Systems. *J. Chem. Phys.* **1993**, *98*, 10089−10092.
(53) Nose, S. A Unified Formulation of the Constant Temperature Molecular-Dynamics Methods. *J. Chem. Phys.* **1984**, *81*, 511−519.
(54) Hoover, W. G. Canonical Dynamics - Equilibrium Phase-Space Distributions. *Phys. Rev. A: At., Mol., Opt. Phys.* **1985**, *31*, 1695−1697.
(55) Brunger, A. T.; Adams, P. D.; Clore, G. M.; DeLano, W. L.; Gros, P.; Grosse-Kunstleve, R. W.; Jiang, J. S.; Kuszewski, J.; Nilges, M.; Pannu, N. S.; Read, R. J.; Rice, L. M.; Simonson, T.; Warren, G. L. Crystallography & Nmr System: A New Software Suite for Macromolecular Structure Determination. *Acta Crystallogr., Sect. D: Biol. Crystallogr.* **1998**, *54*, 905−921.
(56) Wells, D. B.; Belkin, M.; Comer, J.; Aksimentiev, A. Assessing Graphene Nanopores for Sequencing DNA. *Nano Lett.* **2012**, *12*, 4117−4123.
(57) Wanunu, M.; Dadosh, T.; Ray, V.; Jin, J. M.; McReynolds, L.; Drndic, M. Rapid Electronic Detection of Probe-Specific Micrornas Using Thin Nanopore Sensors. *Nat. Nanotechnol.* **2010**, *5*, 807−814.
(58) Kowalczyk, S. W.; Grosberg, A. Y.; Rabin, Y.; Dekker, C. Modeling the Conductance and DNA Blockade of Solid-State Nanopores. *Nanotechnology* **2011**, *22*.31510110.1088/0957-4484/22/31/315101
(59) Plesa, C.; Ananth, A. N.; Linko, V.; Gulcher, C.; Katan, A. J.; Dietz, H.; Dekker, C. Ionic Permeability and Mechanical Properties of DNA Origami Nanoplates on Solid-State Nanopores. *ACS Nano* **2014**, *8*, 35−43.
(60) Hernandez-Ainsa, S.; Misiunas, K.; Thacker, V. V.; Hemmig, E. A.; Keyser, U. F. Voltage-Dependent Properties of DNA Origami Nanopores. *Nano Lett.* **2014**, *14*, 1270−1274.
(61) Aksimentiev, A.; Schulten, K. Imaging Alpha-Hemolysin with Molecular Dynamics: Ionic Conductance, Osmotic Permeability, and the Electrostatic Potential Map. *Biophys. J.* **2005**, *88*, 3745−3761.
(62) Essmann, U.; Perera, L.; Berkowitz, M. L.; Darden, T.; Lee, H.; Pedersen, L. G. A Smooth Particle Mesh Ewald Method. *J. Chem. Phys.* **1995**, *103*, 8577−8593.
(63) Meller, A.; Nivon, L.; Brandin, E.; Golovchenko, J.; Branton, D. Rapid Nanopore Discrimination between Single Polynucleotide Molecules. *Proc. Natl. Acad. Sci. U. S. A.* **2000**, *97*, 1079−1084.
(64) Krishnakumar, P.; Gyarfas, B.; Song, W. S.; Sen, S.; Zhang, P. M.; Krstic, P.; Lindsay, S. Slowing DNA Trans Location through a Nanopore Using a Functionalized Electrode. *ACS Nano* **2013**, *7*, 10319−10326.
(65) Feng, J. D.; Liu, K.; Bulushev, R. D.; Khlybov, S.; Dumcenco, D.; Kis, A.; Radenovic, A. Identification of Single Nucleotides in Mos2 Nanopores. *Nat. Nanotechnol.* **2015**, *10*, 1070−1076.

DOI: 10.1021/acsami.6b11001
ACS Appl. Mater. Interfaces 2017, 9, 92−100